

**Mono-N-oxidation of Heterocycle-Fused Pyrimidines**

Journal:	<i>Dalton Transactions</i>
Manuscript ID	DT-ART-09-2020-003260.R1
Article Type:	Paper
Date Submitted by the Author:	17-Dec-2020
Complete List of Authors:	Shreeve, Jean'ne; University of Idaho, Department of Chemistry Tang, Yongxing; University of Idaho, Chemistry Li, Kejia; Nanjing University of Science and Technology, Chemistry Chinnam, Ajay; University of Idaho, Chemistry Staples, Richard; Michigan State University, Chemistry

ARTICLE

Mono-N-oxidation of Heterocycle-Fused Pyrimidines

Yongxing Tang,^{*†a,b} Kejia Li,^{†a} Ajay Kumar Chinnam,^b Richard J. Staples,^c and Jean'ne M. Shreeve^{*b}Received 00th January 20xx,
Accepted 00th January 20xx

DOI: 10.1039/x0xx00000x

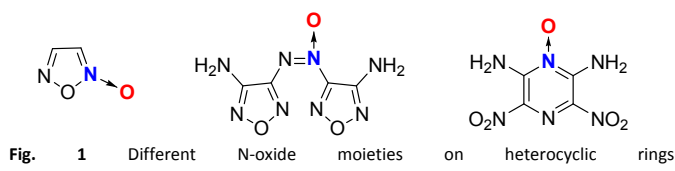
Three nitrogen-rich heterocyclic compounds containing the diamino-pyrimidine mono-N-oxide moiety were synthesized via mild oxidation reactions. Oxidation of the furazano-pyrimidine compound (**1**) with a mixture of trifluoroacetic anhydride (TFAA) and hydrogen peroxide (50%) gave the nitrate salt (**3**). All of the compounds were characterized by NMR spectra, elemental analysis, and single-crystal X-ray diffraction. They show high thermal stability and good detonation performance as well as low sensitivity.

Introduction

Heterocyclic N-oxides have been widely used as structural motifs in various fields such as pharmaceutical agents, functional organic compounds, ligands and energetic materials.¹⁻⁶ In the field of energetic materials, the N-oxide moiety which is another source of oxygen and possible replacement for the nitro group has attracted more and more attention.⁷ Introducing this functionality can improve density, heat of formation and oxygen balance while enhancing detonation performance. Additionally, compared with nitro organic explosives, the N-oxide moiety can delocalize the molecule and reduce mechanical sensitivity.⁸⁻¹¹

In recent years, many N-oxide formation reactions have been reported, such as the formation of the furoxan ring,¹²⁻¹⁴ azoxy link,^{15,16} and N-oxidation on nitrogen-rich heterocyclic compounds¹⁷ (Fig. 1). Some oxidants such as hydrogen peroxide, trichloroisocyanuric acid (TCAA), *m*-chloroperoxybenzoic acid (*m*CPBA), and Oxone have been proved to be effective for N-oxide formation. However, these N-oxidation reactions have focused mostly on single ring or bicyclic rings,¹⁸⁻²⁰ which only require mild oxidants. For fused heterocyclic compounds, strong oxidants such as HOF/CH₃CN are necessary because of the low reactivity of the nitrogen atom in conjugated fused compounds.²¹⁻²³ Likely because of this, the introduction of the N-oxide moiety into fused heterocyclic compounds is still limited.

As a result of the absence of such materials and our continuing interest in the synthesis of fused compounds with the N-oxide moiety, a strategy was developed for the mild oxidation reactions of several nitrogen-rich fused pyrimidine



rings (**1**, **4**, **6**) which give energetic fused mono-N-oxides (**2**, **5**, **7**). All of them have high decomposition temperatures, low sensitivities (> 40 J, > 360 N) and good detonation performances. Additionally, the site selectivity for N-oxidation of fused pyrimidine was investigated theoretically.

Results and discussion

Synthesis

The initial fused compound (**1**) was prepared based on the literature.²⁴ Compounds **4** and **6** are commercially available. The initial investigation for the introduction of the N-oxide moiety began with **1**, which was treated with a mixture of 50% hydrogen peroxide and acetic anhydride at room temperature for 24 h. However, only the starting material (**1**) was recovered. Surprisingly, the mono-N-oxide product (**2**) was isolated in high yield (63%) when the reaction temperature was raised to 50 °C for 1.5 h (Scheme 1). The structure of **2** is supported by single-crystal X-ray diffraction analysis. However, the introduction of more than one N-oxide group failed when the reaction time was extended. Other oxidants such as *m*-chloroperoxybenzoic acid (*m*CPBA) and 12% sodium hypochlorite (NaClO) were also examined for the oxidation of **1**. *m*CPBA was found to be an effective oxidant when reacted with **1** in acetonitrile at reflux for 2 h to give **2** in good yield (70%).

An attempt to oxidize **1** using a mixture of 50% hydrogen peroxide and trifluoroacetic anhydride at room temperature for 1 h led to the formation of a nitrate salt (**3**) in a low yield (16%). However, no product was obtained if the reaction time was extended to 2 h. The nitrate salt (**3**) was also prepared in a high yield (85%) by reacting **1** with 15% nitric acid.

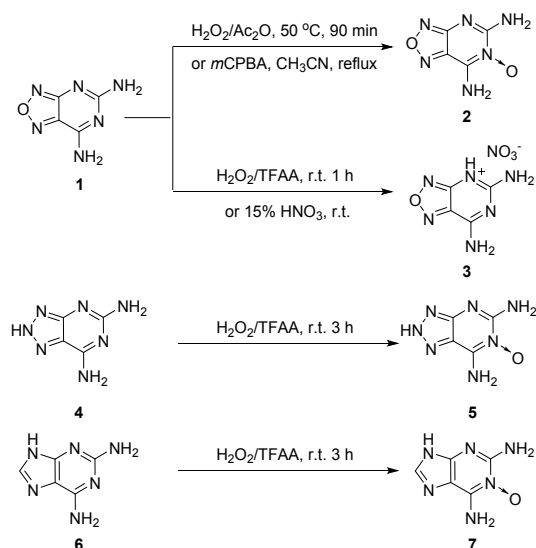
^a Nanjing University of Science and Technology, Nanjing, 210094 China. E-mail: yongxing@njust.edu.cn

^b Department of Chemistry, University of Idaho, Moscow, Idaho, 83844-2343 USA. Fax: (+1) 208-885-5173 E-mail: jshreeve@uidaho.edu

^c Department of Chemistry, Michigan State University, East Lansing, Michigan 48824

† These authors contributed equally to this work.

Electronic Supplementary Information (ESI) available: Crystal structure analysis and NMR spectra. CCDC 2040720-2040723. See DOI: 10.1039/x0xx00000x



Scheme 1 Synthesis of compounds 2, 3, 5 and 7

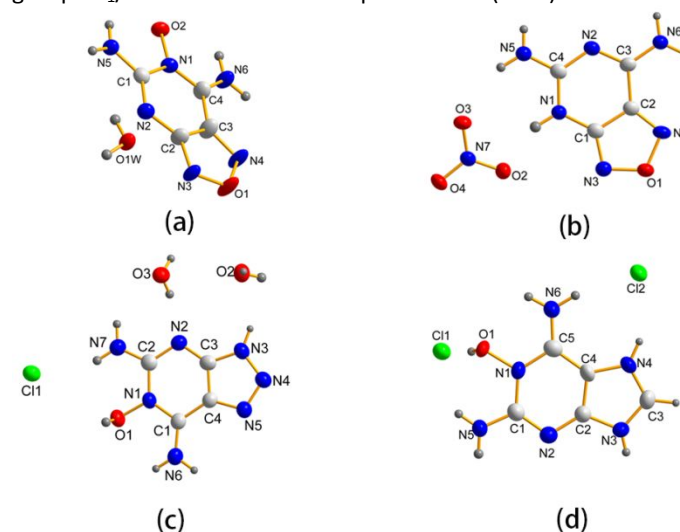
Attempted reactions of 5,7-diamino-2H-[1,2,3]triazolo[4,5-d]pyrimidine (**4**) and 2,6-diamino-9H-purine (**6**) with a mixture of 50% hydrogen peroxide and acetic anhydride gave only unreacted starting materials. However, when a mixture of H₂O₂ (50%) and trifluoroacetic anhydride (TFAA) was used, the mono N-oxide derivatives **5** and **7** were obtained. Compound **5** was characterized with ¹H and ¹³C NMR spectra as well as elemental analysis. Compound **7** was characterized with ¹H NMR and elemental analysis. The ¹³C NMR spectrum was not obtained due to its poor solubility even in *d*₆-DMSO. To confirm the structures of **5** and **7**, the crystal structures of their hydrochloride salts were obtained.

Crystal structure

Compound **2**·H₂O crystallizes in the tetragonal space group P₄₂/n with eight molecules per unit cell (*Z* = 8). The molecular structure is shown in Fig. 2a. Due to the presence of water molecules, the calculated crystal density is 1.448 g cm⁻³ at 100 K. The fused-ring shows a planar structure that is supported by the torsion angles of N2-C2-C3-N4 = 179.7(3)° and N3-C2-C3-C4 = 179.8(3)°. The bond length of N1-O2 is 1.342(2) Å, which is comparable to those in ICM-102.¹⁹ The bond length of C2-C3 is 1.415(3) Å. Due to the presence of the N-oxide moiety and amino groups as well as water molecules in the crystal of **2**·H₂O, six kinds of hydrogen bonds between oxygen atoms and nitrogen atoms were observed. The detailed information is given in the ESI.

Compound **3** crystallizes in the monoclinic space group P2₁/n with a high calculated crystal density of 1.859 g cm⁻³ at 100 K. At 273 K, the density is 1.812 g cm⁻³ according to the volume expansion equation ($\rho_{273K} = \rho_r / (1 + \alpha_v(273 - T))$; $\alpha_v = 1.5 \times 10^{-4} \text{ K}^{-1}$)²⁵. The crystal structure is shown in Fig. 2b. The bond lengths of C4-N5 and N6-C3 are 1.306(2) and 1.312(2) Å, respectively, which are close to the C-amino bond lengths in **2**·H₂O. From the packing diagram in Fig. S2, it is seen that intermolecular hydrogen bonds are formed, such as N1-H1...O2 and N6-H6A...O3.

Compound **5**·HCl·2H₂O crystallizes in the monoclinic space group P2₁/n with four molecules per unit cell (*Z* = 4). The

Fig. 2 a) Molecular structure of **2**·H₂O. b) Molecular structure of **3**. c) Molecular structure of **5**·HCl·2H₂O. d) Molecular structure of **7**·2HCl.

molecular structure is shown in Fig. 2c. As can be seen, the protonation of **5** has occurred at the oxygen atom (O1). The bond length of N1-O1 is 1.377(2) Å, which is longer than that in **2**·H₂O, while the bond length (1.382(3) Å) of C3-C4 is a little shorter. As expected, the fused cation is a nearly planar structure with the torsion angles of N2-C3-C4-N5 = -179.75(18)° and N3-C3-C4-C1 = -179.16(17)°. In the packing diagram (Fig. S3), the fused cations form a layer-by-layer stacking structure with a distance of 3.21 Å. In addition, extensive hydrogen bonds are also found among the fused cation, chloride and water molecules.

Compound **7**·2HCl crystallizes in the triclinic space group P-1 with two molecules per unit cell (*Z* = 2). As depicted in Fig. 2d, the molecule is protonated at both oxygen atom (O1) and nitrogen atom (N4). The bond length of N1-O1 is 1.385(3) Å, which is close to that in **5**·HCl·2H₂O. The bond length of C2-C4 is 1.384(4) Å. Because of the planar structure of the fused cation, they are stacked with π - π interactions with a separation of 3.01 Å (Fig. S4).

Physicochemical and energetic properties

A noteworthy feature of the oxidation reaction of the nitrogen-rich fused pyrimidine ring is the site-selectivity in favor of the introduction of the N-oxide moiety at the position between the two C-amino groups. To better understand the selectivity, density functional theory (DFT) calculations and orbital-weighted dual descriptor for the oxidation were employed.²⁶ In Fig. 3, the green region and the blue region represent positive and negative isosurfaces, respectively. In addition, positive/negative values represent electrophilic/nucleophilic attack susceptibility. It is seen that the positive isosurface distributes around the nitrogen atom between the two C-amino groups, indicating that this position is easily attacked by an electrophilic reagent. Therefore, the N \rightarrow O bond was formed since the active oxygen seeks electrons as an electrophilic reagent. These results account for the

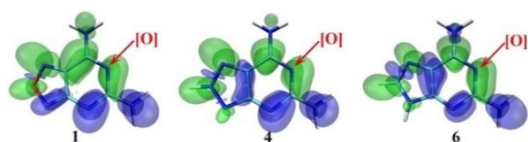


Fig. 3 The orbital-weighted dual descriptor isosurfaces (value = +0.001 and -0.002), using a width of the Gaussian function (Δ) of 0.01 a.u. for **1**, **4** and **6** at the b3lyp/6-31+g(d,p) level.

experimentally observed selectivity that favors the position between the two C-amino groups.

The thermal behavior of the four compounds was determined by differential scanning calorimetry (DSC) at a heating rate of $5\text{ }^{\circ}\text{C min}^{-1}$. The neutral fused-ring compounds show excellent thermal stabilities ($> 280\text{ }^{\circ}\text{C}$). Among them, **7** exhibits the highest decomposition temperature at $309\text{ }^{\circ}\text{C}$, while the decomposition temperatures (onset) of **2** and **5** are $280\text{ }^{\circ}\text{C}$ and $303\text{ }^{\circ}\text{C}$, respectively. The nitrate salt **3** also has a high decomposition temperature (onset) of $247\text{ }^{\circ}\text{C}$. Considering the high decomposition temperatures, they may have potential applications in heat-resistant explosives ($T_d > 250\text{ }^{\circ}\text{C}$).

The gas-phase heats of formation were calculated based on G2 method. The solid-state heats of formation were obtained by subtracting the enthalpy sublimation from the gas phase heats of formation.²⁷ The results are given in Table 1. All of the compounds have positive heats of formation. The densities were measured by using a gas pycnometer at room temperature. Compound **2** has a density of 1.80 g cm^{-3} , while its nitrate salt (**3**) has a slightly higher density of 1.82 g cm^{-3} .

Using the measured densities and the calculated heats of formation, the detonation velocity (v_D) and the detonation pressure (P) was evaluated using EXPLO5 v6.05.02 program.²⁸ Among them, the nitrate salt (**3**) shows the highest detonation properties with a detonation velocity of 8563 m s^{-1} and a detonation pressure of 30.1 GPa , which are a slightly better than those of traditional insensitive energetic materials (TATB and LLM-105). In addition, according to the values of the impact sensitivities and friction sensitivities ($IS: > 40\text{ J}$; $FS: > 360\text{ N}$), they are impact and friction insensitive, indicating they have potential application as insensitive energetic materials.

Table 1 Physiochemical and energetic properties of the compounds and comparison with TNT, TATB and LLM-105.

Compounds	T_d ^{a)} [$^{\circ}\text{C}$]	ρ ^{b)} [g cm^{-3}]	$\Delta_f H$ ^{c)} [kJ/g]	v_D ^{d)} [m s^{-1}]	P ^{e)} [GPa]	IS ^{f)} [J]	FS ^{g)} [N]
2	280	1.80	1.27	7696	21.7	>40	>360
3	247	1.82	1.61	8563	30.1	>40	>360
5-H₂O	303	1.72	0.58	7854	21.5	>40	>360
7	309	1.66	0.47	6609	13.9	>40	>360
TNT ^{h)}	295	1.654	-0.26	6824	19.4	15	>353
TATB ^{h)}	350	1.94	-0.60	8201	28.0	50	>360
LLM-105 ^{h)}	342	1.913	-0.06	8498	30.6	20	360
FOX-7	220	1.845	-0.91	8613	31.6	24.7	>360

a Thermal decomposition temperature (onset) under nitrogen gas (DSC, $5\text{ }^{\circ}\text{C/min}$). b Measured densities, gas pycnometer at room temperature. c Calculated heat of formation. d Calculated detonation velocity. e Calculated detonation pressure. f Impact sensitivity. g Friction sensitivity. h Ref. 28.

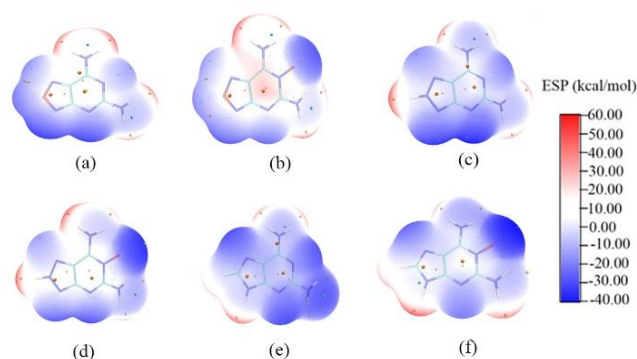


Fig. 4 Electrostatic potential (ESP) of (a) **1**, (b) **2**, (c) **4**, (d) **5**, (e) **6**, (f) **7**

Molecular electrostatic potential (ESP) is a very useful descriptor in understanding reactive sites for electrophilic/nucleophilic reactions and sensitivities since it is related to the electron density. The negative (blue) regions are related to electrophilic reactivity and the positive (red) ones to nucleophilic reactivity. As is shown in Figs. 4a, 4c, 4e, the negative (blue) regions were mainly localized on the nitrogen and oxygen atoms. Considering the actual nitrogen oxidation reaction, it is focused on the two nitrogen atoms on the pyrimidine. In comparing **1** (Fig. 4a) with **2** (Fig. 4b), the introduction of N-oxide makes the blue region more negative, indicating that the less negative nitrogen atoms (between the two C-amino groups) were easily attacked by active oxygen. In addition, for **2** (Fig. 4b), **5** (Fig. 4d) and **7** (Fig. 4f), all negative regions are much larger than the positive regions, suggesting that they are insensitive.

Conclusions

In conclusion, an efficient synthesis of the nitrogen-rich fused diamino pyrimidine mono-N-oxide moiety has been achieved. The reactive site for N-oxidation was studied by theoretical calculation and supported by experimental results. The oxidation of furazan fused diamino pyrimidine with a mixture of TFAA and $50\%\text{ H}_2\text{O}_2$ gives a nitrate salt. The structures were confirmed by single-crystal X-ray diffraction analysis. All of the compounds have high decomposition temperatures and they are insensitive to impact and friction ($IS > 40\text{ J}$, $FS > 360\text{ N}$). The nitrate salt (**3**) has properties comparable with TATB. Furthermore, the N-oxidation reaction of the fused compound will be very useful in the design of new energetic compounds and other heterocyclic compounds.

Experimental section

Caution! Those compounds with mono-oxides are potential energetic materials that might explode under certain conditions such as impact, friction or electric discharge. Appropriate safety precautions including safety goggles, face shields and gloves should always be used all the time.

General

All reagents were purchased in analytical grade and were used as supplied. ^1H and ^{13}C NMR spectra were recorded on a Bruker AVANCE 300 nuclear magnetic resonance spectrometer. Chemical shifts for ^1H and ^{13}C NMR spectra are given with respect to external $(\text{CH}_3)_4\text{Si}$ (^1H and ^{13}C). $[\text{D}_6]\text{DMSO}$ was used as a locking solvent unless otherwise stated. The thermal behaviors were determined by using a dry nitrogen gas purge and a heating rate of $5\text{ }^\circ\text{C min}^{-1}$ on TA Instruments Q2000. IR spectra were recorded using KBr pellets with Thermo Nicolet AVATAR 370. Density was determined at room temperature by employing a Micromeritics AccuPyc II 1340 gas pycnometer. Elemental analyses (C, H, N) were performed with a Vario Micro cube Elementar Analyser. Impact sensitivity were measured by using a standard BAM Fallhammer and friction sensitivity were determined by a BAM friction tester.

Computational Methods

The gas-state enthalpies of formation were calculated based on G2 method. The solid-state heats of formation (for **2**, **5** and **7**) were calculated based on Trouton's rule according to equation (1) (T represents either the melting point or the decomposition temperature when no melting occurs prior to decomposition).²⁷

$$\Delta H_{\text{sub}} = 188/\text{Jmol}^{-1}\text{K}^{-1} \times T \quad (1)$$

For energetic salt (**3**), the solid-phase enthalpy of formation is obtained using a Born–Haber energy cycle.^{30,31}

Crystal Structure Analysis

A yellow needle-shaped crystal (**2**· H_2O) with dimensions $0.20 \times 0.03 \times 0.03\text{ mm}^3$, a colourless plate-shaped crystal (**3**) with dimensions $0.16 \times 0.10 \times 0.04\text{ mm}^3$, a yellow plate-shaped crystal (**5**· $\text{HCl} \cdot 2\text{H}_2\text{O}$) with dimensions $0.21 \times 0.15 \times 0.05\text{ mm}^3$, and a colourless needle-shaped crystal (**7**· 2HCl) with dimensions $0.17 \times 0.05 \times 0.02\text{ mm}^3$ were mounted on a nylon loop with paratone oil. Data were collected using a XtaLAB Synergy, Dualflex, HyPix diffractometer equipped with an Oxford Cryosystems low-temperature device, operating at $T = 100.00(10)\text{ K}$. The structures were solved with the ShelXT³² solution program using dual methods and by using Olex2 1.3-alpha³³ as the graphical interface. The model was refined with ShelXL 2018/3³⁴ using full matrix least squares minimisation on F^2 .

Synthesis

Synthesis of 2

Method a: Hydrogen peroxide (50%, 2 mL) was added dropwise to acetic anhydride (5 mL) at $0\text{ }^\circ\text{C}$. Compound **1** (0.34 g, 2.0 mmol) was added to the solution and the reaction mixture heated and stirred at $50\text{ }^\circ\text{C}$ for 90 min. The precipitate (**2**) (0.21 g, 63%) was collected by filtration, washed with water (10 mL) and dried in air.

Method b: *m*-Chloroperoxybenzoic acid (*m*CPBA, 1.5 g) was added to a suspension of compound **1** (0.40 g, 2.4 mmol) in acetonitrile (20 mL), then the reaction mixture was refluxed for 3 h. The light-yellow solid (**2**) (0.28 g, yield: 70%) was collected by filtration, washed with acetonitrile (10 mL) and diethyl ether (10 mL), dried in air.

2: Light-yellow solid. $T_{\text{d(onset)}}$: $280\text{ }^\circ\text{C}$. $^1\text{H NMR}$ (d_6 -DMSO): δ 9.31 (s, 2H), 8.65 (s, 1H), 8.08 (s, 1H) ppm. $^{13}\text{C NMR}$ (d_6 -DMSO): δ 154.5, 153.7, 141.1, 135.0 ppm. IR (KBr): $\tilde{\nu} = 3353, 1650, 1617,$

1500, 1433, 1373, 1294, 1228, 1159, 1080, 1016, 907, 874, 858, 798, 759, 707, 628 cm^{-1} . Elemental analysis for $\text{C}_4\text{H}_4\text{N}_6\text{O}_2$ (168.11): Calcd C 28.58, H 2.40, N 49.99 %. Found: C 28.59, H 2.54, N 50.13 %.

Synthesis of 3

Method a: Hydrogen peroxide (50%, 1.5 mL) was added dropwise to a solution of trifluoroacetic anhydride (5 mL) in dichloromethane (20 mL) at $0\text{ }^\circ\text{C}$. Then compound **1** (0.50 g, 3.0 mmol) was added to the solution and the reaction mixture was stirred at room temperature for 1 h. After removing the solvent by air, ethanol (10 mL) was added to the residue and the precipitate was collected by filtration. It was washed with ethanol (3 mL) and dried in air. 0.10 g, yield: 16%.

Method b: Compound **1** (0.50 g, 3.0 mmol) was added to nitric acid (15%, 5 mL), the reaction mixture was heated to $50\text{ }^\circ\text{C}$ and stirred for 0.5 h. After removing the dilute nitric acid, the residue was recrystallized with EtOH/ H_2O . 0.55 g, yield: 85%.

3: White solid. $T_{\text{d(onset)}}$: $247\text{ }^\circ\text{C}$. $^1\text{H NMR}$ (d_6 -DMSO): 9.93 (s, 1H), 9.59 (s, 1H), 8.58 (s, 1H), 8.24 (s, 1H) ppm. $^{13}\text{C NMR}$ (d_6 -DMSO): δ 157.7, 154.8, 153.1, 136.0 ppm. IR (KBr): $\tilde{\nu} = 3383, 3336, 3122, 1687, 1585, 1483, 1384, 1289, 1178, 1046, 968, 898, 834, 780, 717, 648, 598\text{ cm}^{-1}$. Elemental analysis for $\text{C}_4\text{H}_5\text{N}_7\text{O}_4$ (215.13): Calcd C 22.33, H 2.34, N 45.58 %. Found: C 22.55, H 2.51, N 45.70 %.

Synthesis of 5·H₂O

Hydrogen peroxide (50%, 1.5 mL) was added dropwise to a solution of trifluoroacetic anhydride (5 mL) in dichloromethane (20 mL) at $0\text{ }^\circ\text{C}$. Then **4** (0.50 g, 3.3 mmol) was added to the solution and the reaction mixture was stirred at room temperature for another 3 h. After removing the solvent by air, water (20 mL) was added to the residue and the solution was neutralized with solid sodium bicarbonate. The precipitate was collected by filtration, washed with water (20 mL) and dried in air.

5·H₂O: (0.37 g, yield: 60%). White solid. T_{m} : $223\text{ }^\circ\text{C}$. $T_{\text{d(onset)}}$: $303\text{ }^\circ\text{C}$. $^1\text{H NMR}$ (d_6 -DMSO): δ 7.59 (s, 1H) ppm. $^{13}\text{C NMR}$ (d_6 -DMSO): δ 153.2, 145.6, 143.7, 118.6 ppm. IR (KBr): $\tilde{\nu} = 3354, 3151, 3017, 1703, 1638, 1618, 1563, 1418, 1392, 1308, 1244, 1214, 1158, 997, 904, 800, 765, 738, 626\text{ cm}^{-1}$. Elemental analysis for $\text{C}_4\text{H}_7\text{N}_7\text{O}_2$ (185.14): Calcd C 25.95, H 3.81, N 52.96 %. Found: C 25.85, H 3.51, N 52.40 %.

Synthesis of 7

Hydrogen peroxide (50%, 1.5 mL) was dropwise added to a solution of trifluoroacetic anhydride (5 mL) in dichloromethane (20 mL) at $0\text{ }^\circ\text{C}$. Then **6** (0.50 g, 3.3 mmol) was added to the solution and the reaction mixture was stirred at room temperature for 3 h. After removing the solvent by air, water (20 mL) was added to the residue and the solution was neutralized with solid sodium bicarbonate. The precipitate was collected by filtration, washed with water (20 mL) and dried in air.

7: (0.30 g, yield: 55%). White solid. $T_{\text{d(onset)}}$: $309\text{ }^\circ\text{C}$. $^1\text{H NMR}$ (d_6 -DMSO): δ 12.60 (br), 8.75 (s, 2H), 7.95 (s, 1H), 7.55 (s, 2H) ppm. $^{13}\text{C NMR}$ (d_6 -DMSO): δ 151.2, 148.4, 147.7, 139.5, 111.0 ppm. IR (KBr): $\tilde{\nu} = 3460, 3130, 2811, 1676, 1625, 1524, 1473, 1415, 1346, 1256, 1202, 1176, 947, 902, 834, 721, 696, 626\text{ cm}^{-1}$. Elemental

analysis for C₅H₆N₆O (166.14): Calcd C 36.15, H 3.64, N 50.58 %. Found: C 35.84, H 3.69, N 50.00 %.

Conflicts of interest

There are no conflicts to declare.

Acknowledgements

Financial support of the Office of Naval Research (N00014-16-1-2089), and the Defense Threat Reduction Agency (HDTRA 1-15-1-0028) is gratefully acknowledged. The Rigaku Synergy S Diffractometer was purchased with support from the National Science Foundation MRI program (1919565). This work was supported by the National Natural Science Foundation of China (21905135), the Natural Science Foundation of Jiangsu Province (BK20190458), the Fundamental Research Funds for the Central Universities (30919011270) and the Large Equipment Open Funding of Nanjing University of Science and Technology.

References

- D. E. Chavez, Energetic Heterocyclic N-Oxides, Springer Berlin Heidelberg, Berlin, Heidelberg, 2017, pp. 1-27.
- Y. Tang, G. H. Imler, D. A. Parrish and J. M. Shreeve, *Org. Lett.*, 2018, **20**, 8039-8042.
- D. Li, P. Wu, N. Sun, Y. Lu, W. Wong, Z. Fang and K. Zhang, *Curr. Org. Chem.*, 2019, **23**, 616-627.
- E. A. Chugunova, V. A. Samsonov, A. S. Gazizov, A. R. Burilov, M. A. Pudovik, and O. G. Sinyashin, *Russ. Chem. B+*, 2018, **67**, 1955-1970.
- Y. Li, C. Qi, S. Li, H. Zhang, C. Sun, Y. Yu and S. Pang, *J. Am. Chem. Soc.*, 2010, **132**, 12172-12173.
- A. M. Mfuh and O. V. Larionov, *Curr. Med. Chem.*, 2015, **22**, 2819-2857.
- P. Politzer and J. S. Murray, *Cent. Eur. J. Energ. Mater.*, 2017, **14**, 3-25.
- J. Yuan, X. Long and C. Zhang, *J. Phys. Chem. A*, 2016, **120**, 9446-9457.
- Y. Tang, C. He, G. H. Imler, D. A. Parrish and J. M. Shreeve, *Chem. –Eur. J.*, 2017, **23**, 15022-15025.
- T. M. Klapötke, J. Stierstorfer and I. Gospodinov, *Eur. J. Org. Chem.*, 2018, **2018**, 1004-1010.
- M. Göbel, K. Karaghiosoff, T. M. Klapötke, D. G. Piercey and J. Stierstorfer, *J. Am. Chem. Soc.*, 2010, **132**, 17216-17226.
- R. Matsubara, H. Kim, T. Sakaguchi, W. Xie, X. Zhao, Y. Nagoshi, C. Wang, M. Tateiwa, A. Ando, M. Hayashi, M. Yamanaka and T. Tsuneda, *Org. Lett.*, 2020, **22**, 1182-1187.
- D. Fischer, T. M. Klapötke and J. Stierstorfer, *Eur. J. Inorg. Chem.*, 2014, **2014**, 5808-5811.
- C. He, Y. Tang, L. A. Mitchell, D. A. Parrish and J. M. Shreeve, *J. Mater. Chem. A*, 2016, **4**, 8969-8973.
- Y. Liu, J. Zhang, K. Wang, J. Li, Q. Zhang and J. M. Shreeve, *Angew. Chem. Int. Ed.*, 2016, **55**, 11548-11551.
- D. Fischer, T. M. Klapötke, M. Reymann and J. Stierstorfer, *Chem. –Eur. J.*, 2014, **20**, 6401-6411.
- H. Wei, H. Gao and J. M. Shreeve, *Chem. –Eur. J.*, 2014, **20**, 16943-16952.
- C. J. Snyder, L. A. Wells, D. E. Chavez, G. H. Imler and D. A. Parrish, *Chem. Commun.*, 2019, **55**, 2461-2464.
- Y. Wang, Y. Liu, S. Song, Z. Yang, X. Qi, K. Wang, Y. Liu, Q. Zhang and Y. Tian, *Nat. Commun.*, 2018, **9**, 2444.
- Y. Liu, G. Zhao, Q. Yu, Y. Tang, G. H. Imler, D. A. Parrish and J. M. Shreeve, *J. Org. Chem.*, 2019, **84**, 16019.
- S. Chen, Y. Liu, Y. Feng, X. Yang and Q. Zhang, *Chem. Commun.*, 2020, **56**, 1493-1496.
- H. Wei, J. Zhang and J. M. Shreeve, *Chem. Asian J.*, 2015, **10**, 1130-1132.
- D. G. Piercey, D. E. Chavez, B. L. Scott, G. H. Imler and D. A. Parrish, *Angew. Chem. Int. Ed.*, 2016, **55**, 15315-15318.
- M. Sako, S. Oda, K. Hirota and G. P. Beardsley, *Synthesis*, 1997, **1997**, 1255-1257.
- J. Zhang, H. Su, S. Guo, Y. Dong, S. Zhang, T. Zou, S. Li and S. Pang, *Crys. Growth Des.* 2018, **18**, 2217-2224.
- T. Lu and F. Chen, *J. Comput. Chem.*, 2012, **33**, 580-592.
- M. S. Westwell, M. S. Searle, D. J. Wales and D. H. Williams, *J. Am. Chem. Soc.*, 1995, **117**, 5013-5015.
- R. Mayer, J. Köhler and A. Homburg, *Explosives*, Wiley-VCH, Weinheim, 2007; 6th edn.
- M. Sućeska, EXPLO5, Version 6.01, Brodarski Institute: Zagreb, Croatia, 2019.
- H. D. B. Jenkins, D. Tudela and L. Glasser, *Inorg. Chem.*, 2002, **41**, 2364.
- H. Gao, C. Ye, C. M. Piekarski and J. M. Shreeve, *J. Phys. Chem. C*, 2007, **111**, 10718.
- G. M. Sheldrick, *Acta Cryst.* 2015, **A71**, 3-8.
- O. V. Dolomanov, L. J. Bourhis, R. J. Gildea, J. A. K. Howard and H. Puschmann, *J. Appl. Cryst.* 2009, **42**, 339-341.
- G. M. Sheldrick, *Acta Cryst.* 2015, **C71**, 3-8.